EIGENVALUE BASED ALTERNANS PREDICTION AND THE EFFECTS OF HEART RATE VARIABILITY ON ALTERNANS FORMATION

A Thesis
SUBMITTED TO THE FACULTY OF
UNIVERSITY OF MINNESOTA
BY

VIRENDRA VILAS KAKADE

IN PARTIAL FULFILLMENT OF THE REQUIREMENTS
FOR THE DEGREE OF
MASTER OF SCIENCE

DR. ALENA TALKACHOVA

June 2013

Acknowledgements

I would like to thank the members of the thesis committee Prof. Hans Othmer and Prof. Murti V. Salapaka for their support in the review of this thesis and agreeing to be members of my Master's defense committee. I would also like to thank all the members of the Talkachova lab and Dr Xiaopeng Zhao at the University of Tennessee for their continual support in my research and review of the research manuscripts.

This work was supported by National Science Foundation [PHY 0957468, PHY 1255410 and CMMI 1233951 to Alena Talkachova, CMMI 1234155 to Xiaopeng Zhao].

Dedication

First and foremost I would like to dedicate this thesis to my advisor Dr. Alena Talkachova for having faith in me in the most difficult of times. Her support and encouragement not only in academic but in other matters as well kept me going and has made me a better individual during the two years at the University of Minnesota. Her mild admonitions kept me from slacking.

Secondly, I would like to thank all the teachers I have had in my life, my parents, grandparents, brother Ravi, sister-in-law Pradnya and my friends (Udayan, Tejas, Harshad, Shreyas, Chaitali, Viren, Anant, Sumedh, Chinmay, Abhishek among many others) for being a constant source of inspiration and support during trying times. They brought out the best in me and tolerated my worst.

Abstract:

Ventricular fibrillation, a leading cause of death in the US, is an instability observed at the whole heart level which may result from the alternation of action potential viz. alternans at the cellular level. Previous approaches to predict alternans formation are based on the slope of the restitution curve which is the relation between the action potential duration (APD) and the duration of the preceding diastolic interval (DI). These approaches propose that alternans exists when the slope of this curve is greater than one and ceases to exist otherwise.

However restitution based approaches have not been successful in all cases. One of the shortcomings of restitution approach is the non-uniqueness of the restitution curve which results from the variety of pacing protocols used to construct it. This has lead to observations in which alternans existed when the slope was less than one and vice a versa. Moreover restitution approaches use just one measurement from each action potential(AP).

Another shortcoming of these approaches is periodic pacing, which is employed to attain the responses (APD and DI) at different basic cycle lengths (BCL) to construct the restitution curve. Upon analysis of electrocardiograms, it is evident that natural pacing is not periodic and exhibits rate variability which can be seen from measurement of RR intervals (which are analogous to BCL) over time.

It would be beneficial to develop a method which is not very related to the restitution approach to predict alternans formation and which would not necessitate the generation of a curve and thus reduce errors introduced due to slope calculation. Such a method could also use multiple measurements from each AP to characterize it. Also, it would be beneficial to study the effects of introducing variability in pacing, on alternans formation. Analysis of such data would give us some valuable insight into the complex phenomenon of alternans.

With these two shortcomings in sight two studies were conducted with specific aims as follows:

Aim1: Apply a dominant eigenvalue method to predict alternans formation in the rabbit heart.

A dominant eigenvalue based alternans prediction was recently developed and tested on data obtained from single cell numerical simulation data. I applied this technique at whole heart level to test whether alternans formation could be predicted using a eigenvalue calculated at each BCL from AP response data. I found that the eigenvalue showed decreasing trend towards the value of -1 as BCL was decreased and approached alternans onset.

Aim2: Study the effect of introducing rate variability in pacing on a ionic model of a single cell.

Ionic model of a single cell was paced using two protocols which introduced variability in the pacing rate by either varying the BCL or DI to test the effects on alternans formation. It was found that introducing variability using first method (varying BCL) lead to alternans formation over wider range of BCL than without variability. The second method (varying DI) however did not give rise to alternans in the model with or without variability.

Table of Contents

List of Tables

List of Figures

List of Abbreviations

Abbreviation	Full Form
DI	Diastolic Interval
APD	Action Potential Duration
AP	Action Potential
BCL	Basic Cycle Length
SCA	Spatial Concordant Alternans
SDA	Spatial Discordant Alternans
VF	Ventricular Fibrillation
LP	Long Perturbation
SP	Short Perturbation
ECG	Electrocardiogram
HRV	Heart Rate Variability
PCA	Principal Component Analysis
TWA	T -Wave Alternans
SS	Steady State

Chapter 1 Introduction

Cardiac action potentials are the responses elicited in cardiac myocytes when excited by an electrical stimulus. These responses can be generated in an isolated cardiac cell by applying an external electric stimulus. However in the heart these stimuli are generated naturally by the pacemaker cells which are a part of the sino-atrial node of the heart, which then propagate through the elaborate conduction system of the heart exciting the cells to which it is connected. These stimuli also propagate through the cell coupling junctions exciting the whole heart in a timely and synchronous manner.

A typical cardiac action potential is illustrated in Fig. 1.1. The peculiar morphology of these APs may be attributed to the various ionic diffusion currents which flow through the cell membrane (K^+,Na^+,Ca^{2+} etc.) and give rise to a trans-membrane potential, which is in fact the AP.

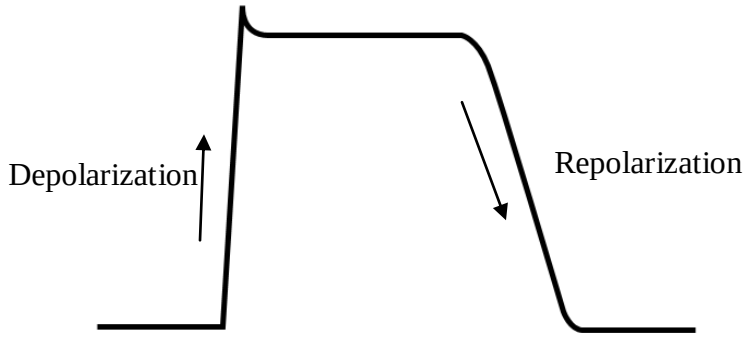

Fig. 1.1 Typical Cardiac Action potential.

In animal heart experiments or in numerical simulations the cardiac tissue under study is excited by stimuli at constant intervals of time which gives rise to the term periodic pacing (refer Fig. 1.2 A). The time difference between two stimuli is called the Basic Cycle Length (BCL). In such experiments the APs are recorded over time at

different BCL values and APD and DI measurements are made. APD measurements can be made at different repolarization levels as illustrated in Fig. 1.2 B.

Also, it is important to note that periodic pacing introduces a relation between these measurements given by Equation 1.1

$$APD_n + DI_n = BCL \qquad \textbf{Equation 1.1}$$

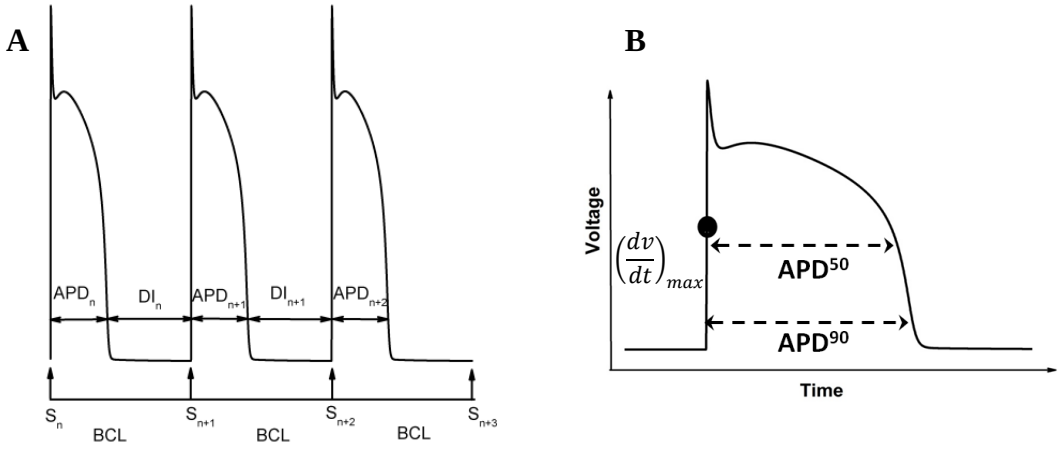

Fig. 1.2 A. Action potentials due to periodic pacing S: Stimulus, DI: diastolic interval, APD: Action potential duration. B. Action potential with 2 different APD measurements and the point of maximum slope $\left(\frac{dv}{dt}\right)_{max}$ represented by black dot.

Usually at higher values of BCL the action potential responses are of equal duration over time, however at lower values of BCL the phenomenon of alternans may result. During this phenomenon the APD alternates as illustrated in Fig. 1.3 which shows APs with short-long-short APDs. Alternans has a complex spatio-temporal organization which means that it does not occur in the entire heart all at once but rather evolves over the surface of the heart over time. Moreover the alternans exhibited at different regions in the heart at the same BCL may be of different (spatially discordant alternans SDA) or same phases (spatially concordant alternans i.e. SCA). Regions out of phase, i.e. exhibiting SDA show short-long-short sequence of APD in one region whereas long-short-long in other and regions showing SCA show same sequence of alternation all over.

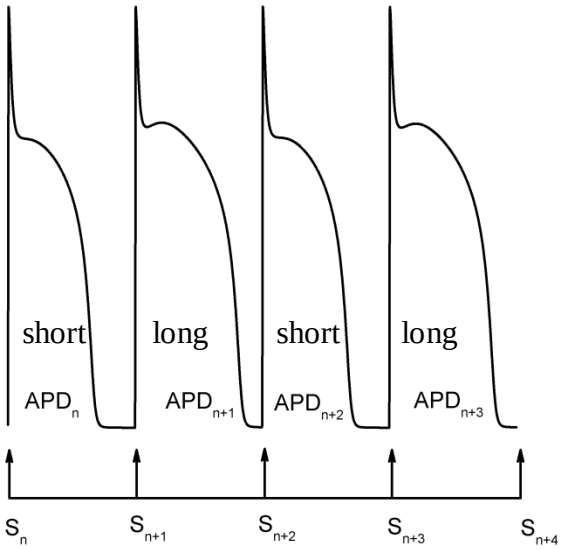

Fig. 1.3 Alternans i.e. an alternation in action potentials over time in a single cell (representative).

This alternans of action potential manifests as repolarization alternans (also referred to as T-wave alternans (**TWA**)) at the tissue and whole heart level and is observed on the ECG. Moreover it is also known that a large variation of AP reflects as a small TWA (at μV level). TWA is often used as a clinical marker of identifying patients at risk of arrhythmias, more specifically TWA also indicates susceptibility of the heart to ventricular fibrillation [1-4] (an instability of the heart) which is one of the leading causes of death in the US [5]. Hence it is of importance to study the formation of alternans using experiments as well as numerical simulations towards an effort to predict its formation.

A common technique for studying the onset of APD alternans is to construct a restitution curve that describes the nonlinear relationship between the APD and preceding diastolic interval (DI) given by the equation below.

$$APD_{n+1} = f(DI_n) \qquad \textbf{Equation 1.2}$$

where the f denotes the curve of restitution and APD_{n+1} is the duration of action potential due to the stimulus number (n+1) and DI_n is the diastolic interval preceding the action potential.

Usually, these restitution curves can be constructed using various pacing protocols in which periodic stimuli are applied at different BCLs and the responses (APD and DI) are measured and plotted to give the restitution curve ultimately. A representative restitution

curve is shown in Fig. 1.4. As shown in the Fig. 1.4 change in APD is small over a large range of values of DI. However at lower DI, APD shortens as well. This phenomenon is called restitution which ensures that the heart has enough time to recover from the action potential and refill with blood.

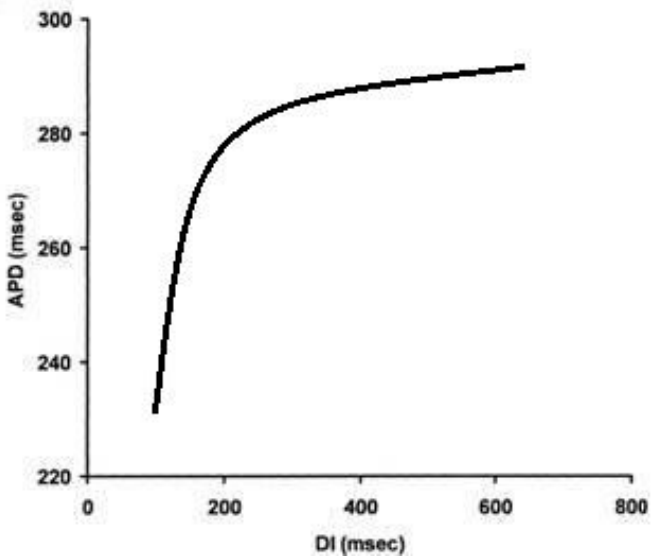

Fig. 1.4 A representative restitution curve.

However this property of the heart, during the application of periodic pacing gives rise to APD alternans at low values of DI. This has been linked to the slope of the dynamic restitution curve being equal to one [6]. The restitution theory also states that alternans may amplify when the slope of restitution exceeds one and gets suppressed when the slope value is less than one as shown in Fig. 1.5 which can be explained by the one dimensional mapping relationship established by Equation 1.2.

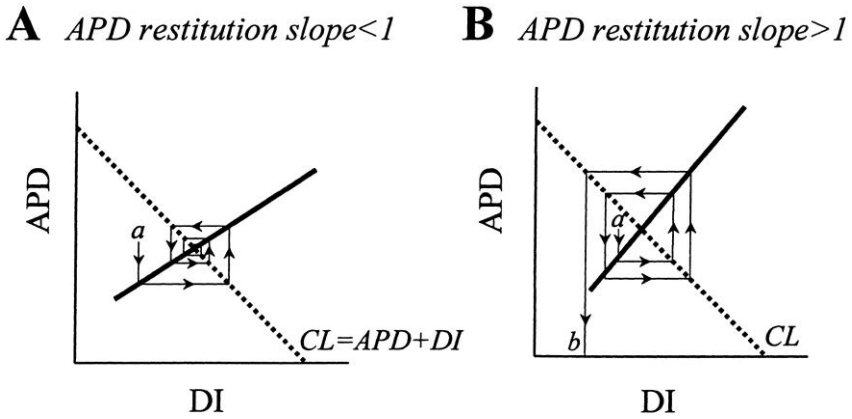

Fig. 1.5 A. Decreasing Alternans when slope is less than 1 B. Increasing Alternans when slope is greater than 1. [37]

However, several experimental studies show that alternans can occur at values of slope less than one [7-10]. Moreover, other experiments show that no alternans is seen even when the slope was greater than one [8, 11, 12]. This failure to predict the onset of alternans using restitution curves has been alluded to several reasons, such as the presence of short term memory which refers to the phenomenon during which the APD depends not just on the preceding diastolic interval but rather on several of the previous intervals that significantly complicates the dynamics of cardiac tissue [7-9, 13-16]. Also, not taking into consideration the intracellular calcium cycling can play a major role in developing APD alternans [13, 17]. Another reason for the failure of the restitution hypothesis is thought to be the complex spatio-temporal formation of APD alternans in the heart where the spatial complexity plays an important role. It has been demonstrated that APD alternans has a local onset in the heart both spatial and temporal, i.e. alternans develops in a small region of the heart, and then occupies the entire surface as the BCL decreases [18].

This thesis focuses of two shortcomings as below:

1. Non-uniqueness of the restitution curve

One shortcoming, as discussed above, in predicting the alternans on the basis of slope of the restitution curve is due to its non-uniqueness attributed to multiple ways of generating the restitution curve resulting out of responses to various pacing protocols.

An approach which is not very related to restitution curve may help alleviate this

shortcoming by basing the prediction on just the APD measurements at each BCL and not on the basis of a curve. Moreover, if this method utilizes multiple measurements from each AP to predict alternans, it would be a good step towards attempting to incorporate the various ion dynamics that shape an AP in alternans prediction.

As alternans is an instability of the heart, one approach to predict its formation could utilize eigenvalues derived from its responses at each BCL using the principle that when the magnitude of eigenvalue of a system exceeds -1 it becomes unstable. Eigenvalues have been used before to determine stability of physiological systems by studying their physical analogues like the swinging heart, analyzed by the forced spring-pendulum [31] and the respiratory control system [32].

Aim1 deals with this shortcoming by utilizing a eigenvalue based approach to predict alternans formation in rabbit hearts.

2.Periodic pacing:

A reason why restitution approach may fail is due to the periodic nature of pacing used in experiments as well as numerical simulations. Such periodic pacing is hardly natural as analysis of clinical electrocardiograms (ECG) suggest that the heart rate is never constant and exhibits heart rate variability (HRV) even over short intervals of time. It would be of interest to study the effects of introducing rate variability in the pacing protocols used in experiments or numerical simulations on alternans formation.

Aim2 improves on this shortcoming by studying effects of HRV on alternans formation in single cell ionic model by numerical simulations.

This thesis tries to improve on above two shortcomings of the restitution approach with two specific aims in mind:

Aim1: Application of dominant eigenvalue method to predict alternans formation in the rabbit heart.

I apply a recently published dominant eigenvalue based alternans prediction technique which was developed to predict alternans formation in a single cell numerical model to data from four optical mapping experiments to test its capability to predict alternans in the whole rabbit heart. Chapter 2 deals with the data, methods and results for this aim.

Aim2: Study the effect of introducing rate variability in pacing on a ionic model of a single cell.

This aim deals with studying the effects of introducing pacing rate variability using two different pacing protocols on the alternans formation in numerical simulations of canine ionic model of a single cell. Chapter 3 deals with the methods and results for this aim.

The theoretical background and technique used for eigenvalue calculation [22] are given in the appendix (Chapter 6) .

Chapter 2 Application of dominant eigenvalue method to predict alternans formation in the rabbit heart.

2.1 Background

An eigenvalue approach [22] was recently developed which models the single cell in state space as a system characterized by various action potential duration measurements. In this approach the cell model is paced at decreasing BCL values until alternans occurs. An eigenvalue is calculated at each BCL based on series of action potential measurements at that BCL and is shown to approach -1 as we approach the BCL corresponding to alternans in a single cell.

This approach is based on the assumption that dominant eigenvalues of a dynamic system, e.g. the heart in our case, can be estimated from transient response of the system after perturbation [19]. Specifically, alternans results from a period-doubling bifurcation, which occurs when a negative eigenvalue approaches -1 [19].

When the underlying model of a cardiac action potential is explicitly available, eigenvalue calculation is straightforward [19] allowing determination of system's stability [20, 21]. On the other hand, stability analysis based on experimental data is more difficult to perform, due to several reasons: the appropriate state variables governing the dynamic system are unknown, or approximations to state space may consist of quantities that cannot be readily measured [20-22].

This new technique [22] estimates the stability of the system from data acquired using numerical simulations, and can be applied to experimental data, which allows calculation of the most dominant eigenvalues from a time series of readily measurable quantities. This technique is based on the principle that when a dynamic system is mildly perturbed from its steady state, only a small number of dominant eigenvalues are associated with it and the most dominant eigenvalues can be found via principal component analysis (PCA) [23]. This technique was validated numerically in [22] **(**refer Fig. 2.1 and Table 2.1**)** where dominant eigenvalues were calculated from time series of action potentials obtained using a Shiferaw-Fox model of a single cardiac myocyte [24, 25].

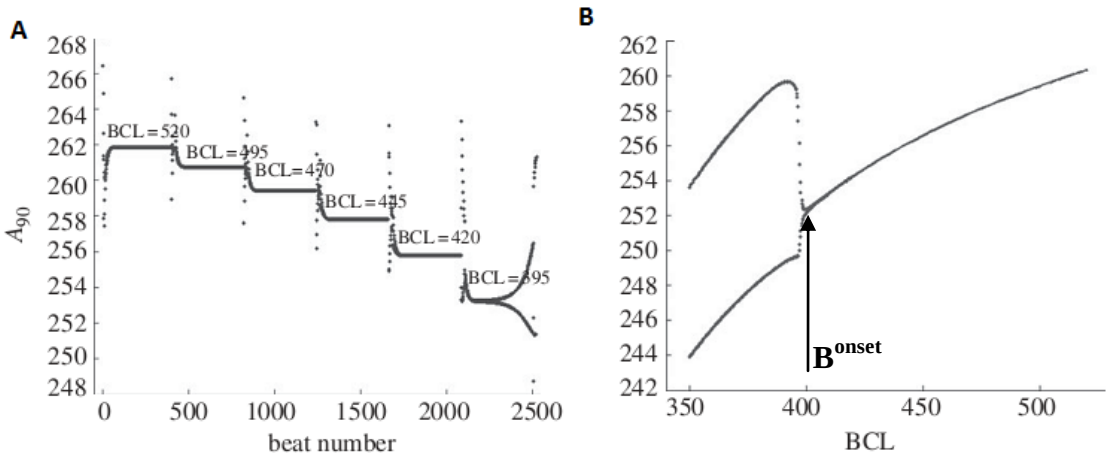

Fig. 2.1 A. The pacing protocol and the corresponding APD values of a cell model at various BCL values. B. The plot of APD values versus the BCL values showing that alternans occurred at BCL close to 400 ms(B^{onset}) [22].

BCL(ms.)	Dominant Negative Eigenvalue
520	-0.637
495	-0.701
470	-0.773
445	-0.851
420	-0.933

Table 2.1 The BCL values and corresponding dominant eigenvalues which show that the negative dominant eigenvalue approached -1 as the BCL was reduced and approached B^{onset} at about 400ms [22].

I applied this technique to optical mapping experimental data at the whole heart level effectively treating each pixel in the optical mapping data as a single cell to derive an average eigenvalue and test whether it is effective in prediction of alternans. In particular two different sets of APD measurements from just 4 APs at each BCL were used to characterize the action potentials and derive corresponding two different eigenvalues and test their efficacy in alternans prediction.

2.2 Data Description

Four optical mapping experiments which recorded the action potential responses from 4 rabbit hearts were made available to me. Each experiment had action potentials

recording for a series of BCL values according to a specific pacing protocol which is explained in section 2.3.2. The technique used for acquiring data viz. optical mapping is also explained in brief in section 2.3.1.

2.3 Methods

This section deals with optical mapping, pacing protocol which was used in the experiments to pace the hearts, measurement of APDs and the actual eigenvalue calculation technique which was then applied to these APD data.

2.3.1 Optical Mapping and Animal Model

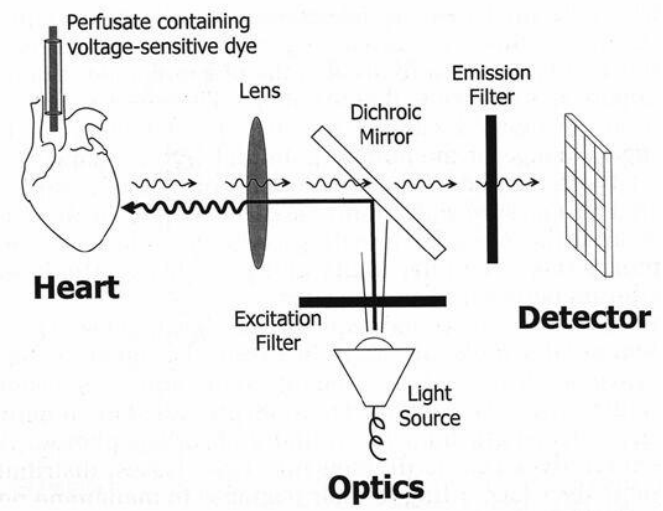

Fig. 2.2 Optical Voltage Mapping setup [34]

Description of Optical Mapping:

Optical mapping is a technique to record the electrical activation in cell, tissue or even organs with the help of voltage sensitive dyes. Optical mapping is even more useful than multisite recording techniques because using the current technology we can map the electrical activity of the entire surface rather than at singular sites leading to visualization of interesting phenomena like the progression of an electrical activation wave-front on the surface of heart.

Voltage sensitive fluorescent dyes are molecules which are able to attach themselves to cell membranes. The amount of fluorescence emitted by these dye molecules is proportional to the trans-membrane voltage of the cell when excited by a light source of constant intensity and wavelength. Thus voltage sensitive dyes act as molecular sensors converting a part of the electrical energy of the cell into light. We can use optical detector like a CCD array to record this fluorescence over a period of time. Tracing any spatial location over time gives us an optical membrane potential which

corresponds to the average electrical activation behavior (action potential) of cells belonging to the region which it maps. Optical mapping enables us to map the entire surface of the organ and hence it is used in the study various arrhythmias resulting out of irregular electrical activity.

Animal Model and Setup:

All experiments were performed according to National Institute of Health and University of Minnesota guidelines. New Zealand White Rabbits of either sex (n=4, 2.5-3 kg) were injected with heparin sulfate (300 U) and anesthetized with sodium pentobarbital (75 mg/kg IV). After thoracotomy, the hearts were quickly removed and immersed in cardiopelgic solution (glucose 280mM, KCl 13.44mM, $NaHCO_3$ 12.6mM, mannitol 34mM). The aorta was quickly cannulated and retrogradely perfused with warm (36 ± 1 °C) oxygenated Tyrode's solution (NaCl 130Mm, $CaCl_2$ 1.8mM, KCl 4mM, $MgCl_2$ 1.0mM, NaH_2PO_4 1.2mM, $NaHCO_3$ 24mM, glucose 5.5mM) under constant pressure (70 mm Hg). The Tyrode's solution's pH was maintained at 7.4 with adjustments made with HCl. The hearts were immersed in a chamber and superfused with the same Tyrode's solution. Blebbistatin (10 µmol/L) was added to the Tyrode's solution to reduce motion artifacts.

A bolus of 5 mL of the voltage sensitive dye Di-4-ANEPPS (10 µmol/L) was injected. This dye was excited with the use of a diode-pumped continuous-excitation green laser (532 nm, 1W, Shanghai Dream Laser Technology Co, China). A charge-coupled device camera (CA-D1-0128T, DALSA, Waterloo, Ontario, Canada) was used to record fluorescence intensity from the right ventricle (RV) of the heart. Movies were acquired at 600 frames per second with a spatial resolution of 64X64 pixels. The background fluorescence was subtracted from each frame. In addition, spatial (3X3 pixels) and temporal (5 pixels) conical convolution filters were used.

2.3.2 Pacing Protocol

External stimuli (5 ms durations, twice the threshold) were applied to the base of the heart using a down-sweep pacing protocol [16] in which steady state BCLs, B^{SS}, were progressively reduced from 300 ms to 130 ms in 10 or 20 ms decrements. The following

steps were applied at each BCL, which are represented in Fig. 2.3 for specific case of B^{SS} = 240 ms:

I. 100 stimuli were applied at B^{SS} to achieve a steady state (SS).
II. 8 stimuli were delivered at B^{SS} to measure the SS response (filled circles).
III. One additional stimulus (long perturbation, LP) was applied at a longer BCL $B^{LP}=B^{SS}+10ms$ (open circle).
IV. 4 stimuli were applied at B^{SS} to return to SS after the LP (open squares).
V. One additional stimulus (short perturbation, SP) was applied at a shorter BCL $B^{SP}=B^{SS}-10ms$ (open circle).
VI. 4 stimuli were applied at B^{SS} to return to SS after the SP (filled squares).

Optical mapping movies (5s duration) were acquired to capture the responses during SS (part II of the pacing protocol), and action potentials after LP and SP (filled and open squares in Fig. 2.3, respectively) at each BCL.

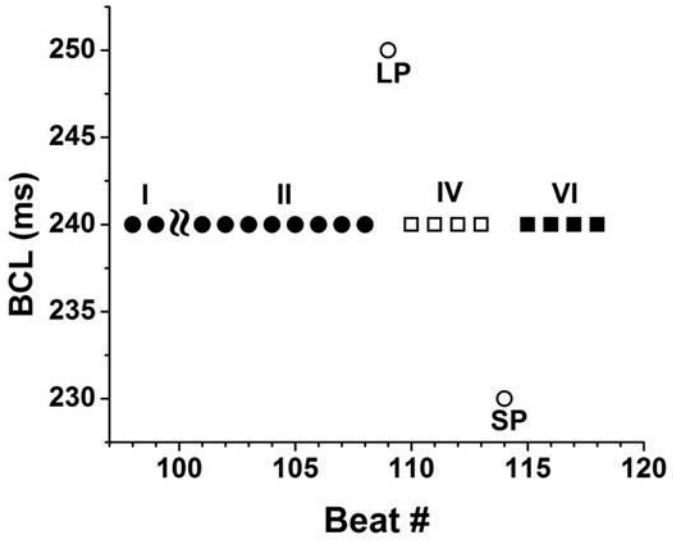

Fig. 2.3 One sequence of pacing protocol for BSS = 240 ms, where different parts of the pacing protocol are shown.

2.3.3 APD and Alternans measurement

At each pixel, the APDs were measured from the maximum slope of depolarization, $(dv/dt)_{max}$ (see dot in Fig 1.2B), to the different levels of action potential repolarization [22]. For instance, Fig. 1.2B shows APD^{90} and APD^{50} measurements.

At each pixel, the magnitude of steady state APD alternans was calculated for responses measured at SS (step II of the pacing protocol) as $|\Delta APD| = |\langle APD_{odd} \rangle - \langle APD_{even} \rangle|$, where $\langle APD_{odd} \rangle$ and $\langle APD_{even} \rangle$ are mean values of APDs calculated from 4 odd and 4 even beats at SS, respectively. The threshold for alternans was set to 5 ms. [18, 30]. The phase of APD alternans was negative for short-long APD sequences (represented by blue) and positive for long-short APD sequences (represented by red).

Two-dimensional (2D) APD maps were constructed for the epicardial surfaces of the heart based on SS responses at each BCL. In the heart, the local spatial onset of alternans, B^{onset}, was defined as BCL at which at least 10% of the surface of the heart was occupied by alternans [18]**.** Two spatial regions of the heart were defined at B^{onset}: the ***1:1***$_{alt}$ region, where alternans was present, and the ***1:1*** region, which exhibited 1:1 behaviour. These two regions were back-projected to all previous BCLs, and the mean values and standard errors for all parameters were calculated and averaged separately for these two regions.

2.3.4 Eigenvalue calculation: λ_2 and λ_4 & Eigenvalue Maps

Eigenvalue calculation was based on the dominant eigenvalue method proposed in [22] **(**The detailed process is given in sections 6.1 & 6.3). Specifically, APDs after SP were considered for eigenvalue estimation for each pixel. (step VI). At each pixel, two different data matrices, $Z_{[4]}$ and $Z_{[2]}$, were populated based on either four (APD^{90}, APD^{70}, APD^{50}, APD^{30}) or two (APD^{90}, APD^{50}) APD measurements from each of the four action potentials after SP, at each BCL as following,

$$Z_{[4]} = \begin{pmatrix} APD_1^{90} - APD_*^{90} & \cdots & APD_1^{30} - APD_*^{30} \\ \vdots & \ddots & \vdots \\ APD_4^{90} - APD_*^{90} & \cdots & APD_4^{30} - APD_*^{30} \end{pmatrix} \quad \textbf{Equation 2.1}$$

and

$$Z_{[2]} = \begin{pmatrix} APD_1^{90} - APD_*^{90} & APD_1^{50} - APD_*^{50} \\ \vdots & \vdots \\ APD_4^{90} - APD_*^{90} & APD_4^{50} - APD_*^{50} \end{pmatrix} \quad \textbf{Equation 2.2}$$

where APD_n^k indicates APD measured at k % of repolarization from the beat number n after SP, where $\mathbf{n} \in [1,4]$. Also APD_*^k indicates the SS response measured at k % of repolarization and calculated as mean of the 8 action potential responses in stage II of the pacing protocol.

$Z_{[4]}$ and $Z_{[2]}$ are used to determine the most dominant eigenvalues $\lambda_{[4]}$ and $\lambda_{[2]}$ respectively for each pixel, at each BCL as per technique described in [22]. This technique uses singular value decomposition to determine the principal dimensions in the above matrices. Least squares method is then applied to the data in these principal dimensions to estimate a matrix, whose eigenvalues are the ones sought (refer sections 6.1 & 6.3). Since some of eigenvalues were complex-valued, only the most negative (or zero) real part of the eigenvalues were used for further analysis. The most negative value of the eigenvalues was restricted to -2.

2D $\lambda_{[4]}$ and $\lambda_{[2]}$ maps were constructed for each BCL, similar to 2D ΔAPD maps. The B^{onset} measurements and information about two regions of the heart, *1:1* and $1{:}1_{alt}$ were taken from the 2D ΔAPD maps and projected to 2D eigenvalue maps. The eigenvalues $\lambda_{[4]}$ and $\lambda_{[2]}$ were used for eigenvalue histogram generation for each BCL, separately for *1:1* and $1{:}1_{alt}$ regions. Mean eigenvalue $\bar{\lambda}_{[4]}$ was calculated for *1:1* and $1{:}1_{alt}$ regions separately at each BCL by averaging the eigenvalues from 2D $\lambda_{[4]}$ maps. Similarly 2D $\lambda_{[2]}$ maps were used to generate $\bar{\lambda}_{[2]}$ values.

Statistical Analysis:

The mean values and standard errors for all parameters were calculated and averaged separately for *1:1* and $1{:}1_{alt}$ regions of the heart. Group data are presented as the mean ± SE. Statistical comparisons between the two regions in the heart were performed using a two-sample *t*-test, and between different rabbits using ANOVA (Origin Software, Northampton, MA). Values of $p < 0.05$ were considered statistically significant.

2.4 Results

2.4.1 Spatiotemporal Evolution of APD alternans and Eigenvalue

In order to observe whether the eigenvalues ($\lambda_{[4]}$) calculated over the heart surface also show a spatiotemporal evolution as was observed with the alternans [18], alternans maps and corresponding eigenvalue maps were also generated by calculating the eigenvalue and alternans value at each pixel, at each BCL.

The spatiotemporal evolution of alternans in the RV of the heart is presented in Fig. 2.4A where 2D ΔAPD alternans maps are shown for different values of BCLs. In Fig. 2.4A, the white color corresponds to 1:1 behavior, and red and blue colors show alternans with different phases. Note that the local onset of APD alternans occurred at BCL B^{onset} = 170 ms (see red box in Fig. 2.4A), and alternans occupied the entire surface of the heart as BCL progressively decreased. Note the formation of spatially discordant alternans (SDA) at lower BCL. The local onset of alternans in the heart has been described in our previous studies [18]. The representative traces from a single pixel at B^{onset} illustrating 1:1 behavior (black) and alternans (blue and red) are shown in Fig. 2.4B.

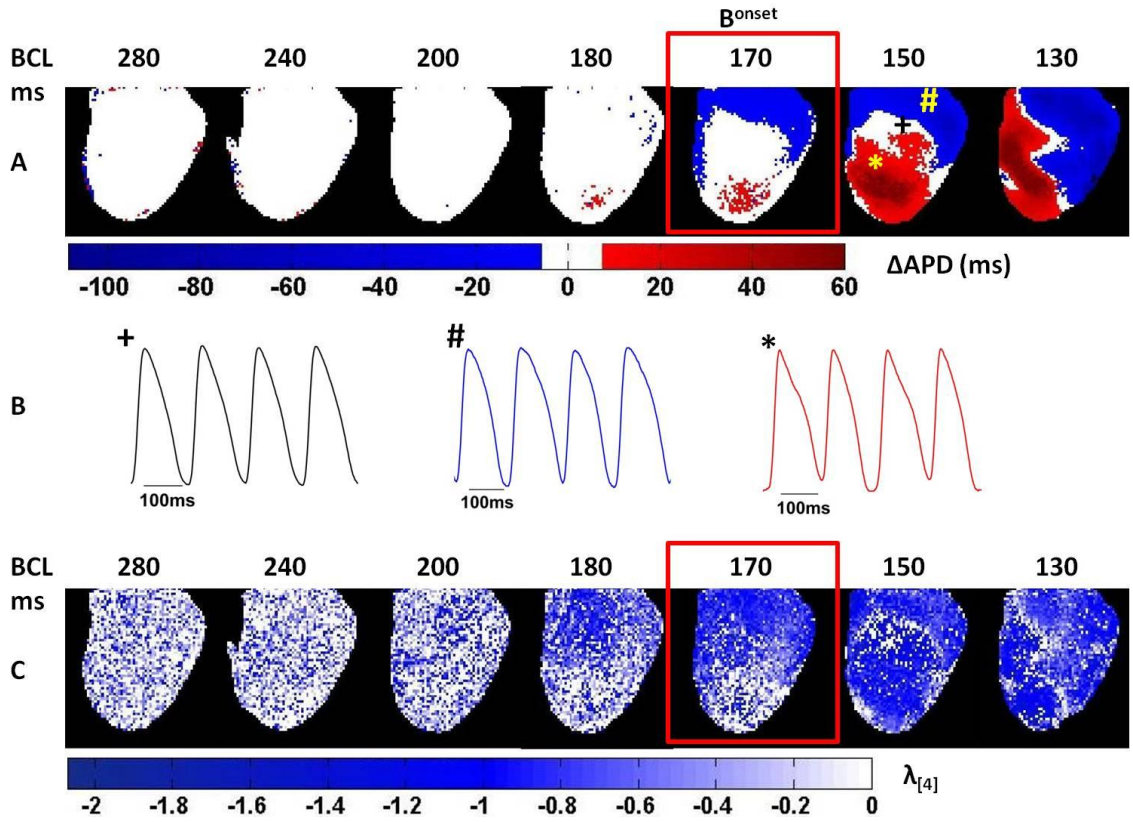

Fig. 2.4 A. 2D ΔAPD maps illustrating spatiotemporal evolution of alternans in the right ventricle of the rabbit heart at different BCLs. The local onset of alternans occurs at B^{onset} and is indicated by a red box. The color bar shows the amplitude of alternans (red or blue) and 1:1 response (white). B. Representative traces of action potentials from three single pixels in Fig. 2.4A demonstrating 1:1 responses (black) and alternans with different phases (red and blue). C. 2D $\lambda_{[4]}$ maps calculated for A at different BCLs, with red box representing the local onset of APD alternans Bonset. The color bar shows the eigenvalues $\lambda_{[4]}$.

Fig. 2.4C represents the spatial distribution of dominant negative eigenvalues $\lambda_{[4]}$ that were calculated using $Z_{[4]}$ matrix, for the same values of BCLs as the 2D ΔAPD maps in Fig. 2.4A. Note that only non-positive $\lambda_{[4]}$ are present and are restricted to [-2, 0] range. The local onset of APD alternans, B^{onset}=170 ms, is shown in Fig. 2.4C as a red box. Note the visual correlation between the APD alternans and $\lambda_{[4]}$ especially at small BCLs.

2.4.2 Correlation of Eigenvalue and APD alternans

Correlation, if any, found between the alternans value and the eigenvalue at any pixel would be a very good finding. Also interesting would be the relation, if any, found between the phase of alternans and the eigenvalue. This correlation was explored by doing a scatter plot of alternans value and the corresponding eigenvalue at particular BCL for regions which showed alternans.

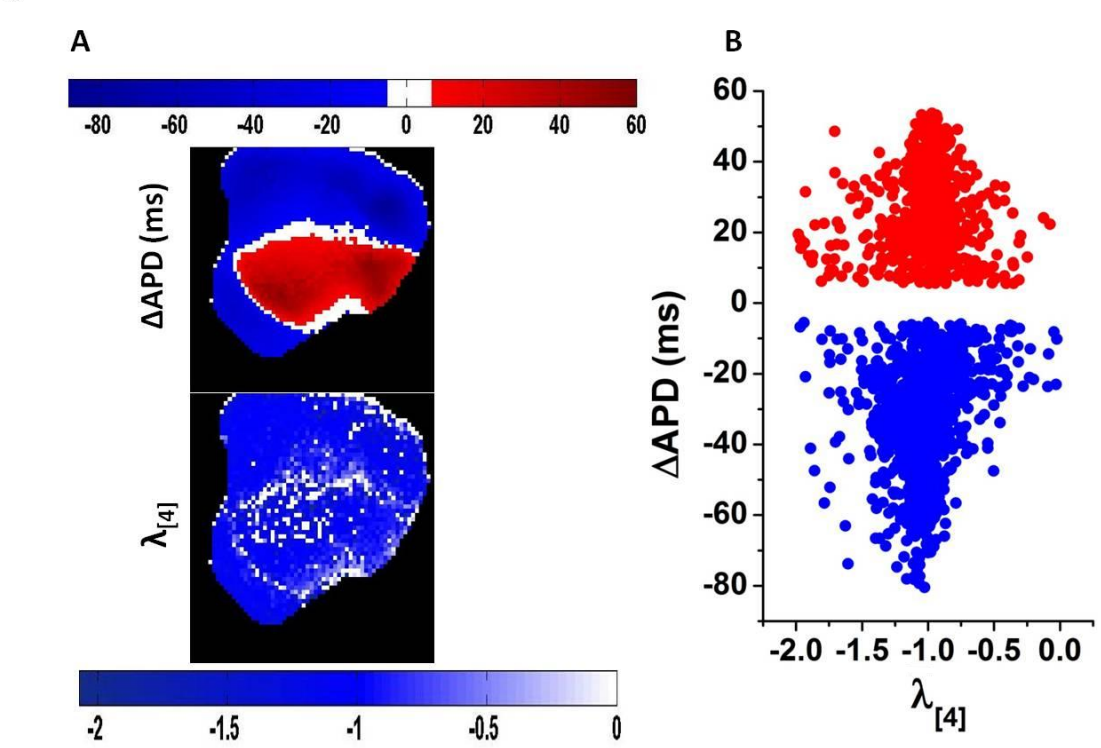

Fig. 2.5 A. 2D ΔAPD map showing the alternans at BCL=150ms. with the color bar (top) and the corresponding 2D $\lambda_{[4]}$ map with its color bar (bottom) for one of the experiments. B. The correlation of eigenvalues of pixels having positive (red) and negative (blue) ΔAPD.

Fig. 2.5A shows the 2D ΔAPD and corresponding $\lambda_{[4]}$ map at BCL=150ms. from a different representative experiment for which the B^{onset} = 180ms. Fig. 2.5B shows the correlation between the amplitude of SDA with different phases (red and blue) and $\lambda_{[4]}$. Note that $\lambda_{[4]}$ has a normal distribution around value of -1 for both phases of SDA suggesting that phase of alternans does not affect the eigenvalue.

2.4.3 Eigenvalue histograms at different BCLs

Alternans formation in the heart is a complex spatio-temporal phenomenon and to predict it on the basis of eigenvalue, it is necessary to check how the eigenvalues in the two regions which exhibit ($1{:}1_{alt}$) and don't exhibit (1:1) alternans at B^{onset} evolve over various BCLs preceding it. This could be done by observing the eigenvalue histograms in these two regions at each BCL.

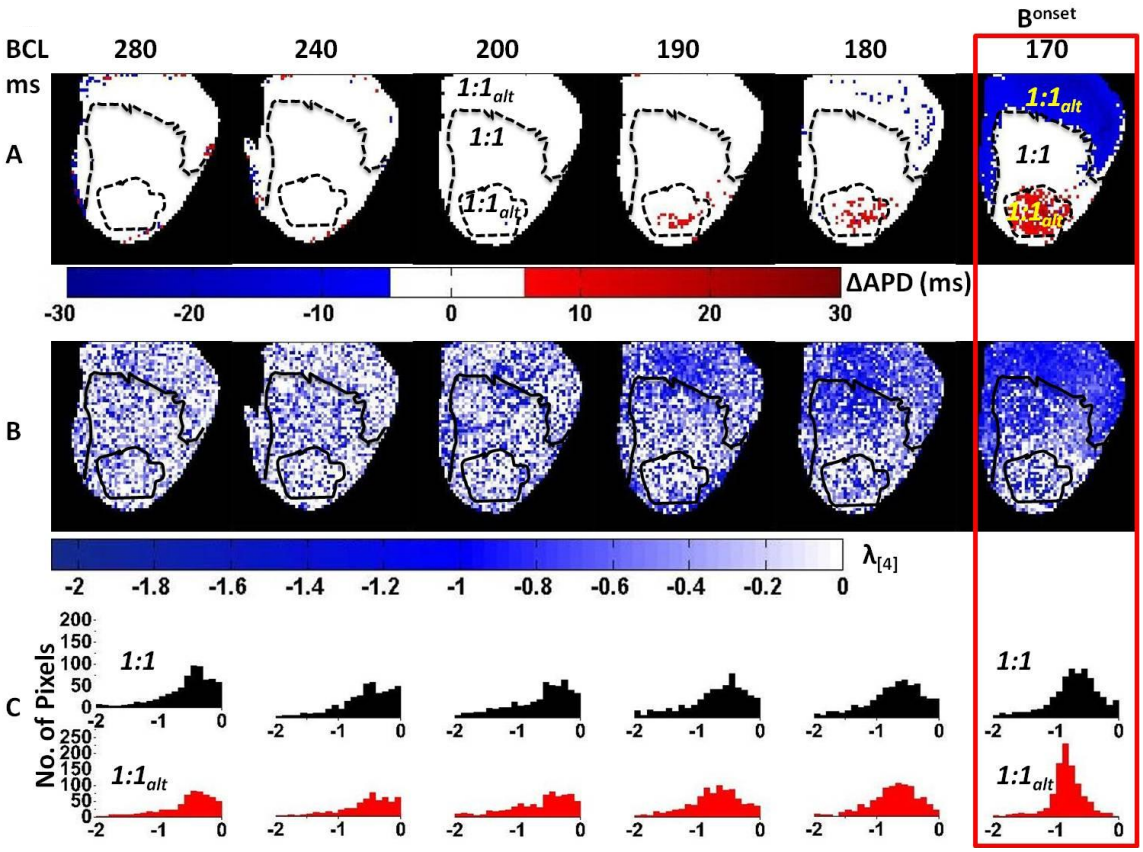

Fig. 2.6 A. 2D ΔAPD maps illustrating the evolution of alternans in the right ventricle of rabbit heart until its onset at BCL=170ms (marked by red box) with the regions exhibiting alternans at Bonset back-projected on preceding BCLs (dashed black lines). The color bar represents the amplitude of alternans (red or blue) and 1:1 response (white). B. 2D $\lambda_{[4]}$ maps calculated for A with the regions showing alternans at Bonset in A marked by (solid black lines). The color bar shows the eigenvalues $\lambda_{[4]}$. C. Eigenvalue histograms derived from B corresponding to the pixels belonging to the 1:1 (black histogram) and 1:1alt (red histogram) regions at each BCL showing the gradual concentration of the histogram for the 1:1alt region around the eigenvalue of -1 with decreasing BCL.

Fig. 2.6A shows the definitions of *1:1* and $1{:}1_{alt}$ regions of the heart for the 2D ΔAPD maps from the experiment illustrated in Fig. 2.4A. Specifically, at the spatial local onset of alternans, i.e. at BCL B^{onset} = 170 ms, the region without alternans (*1:1*) and the region with alternans ($1{:}1_{alt}$) are defined (see black dashed outlines) and back-projected on the previous BCLs. Fig. 2.6B shows corresponding 2D $\lambda_{[4]}$ maps calculated using the $Z_{[4]}$ matrix. The *1:1* and $1{:}1_{alt}$ regions on the 2D $\lambda_{[4]}$ maps are taken from the 2D ΔAPD maps to visually illustrate the spatial distribution of eigenvalues in these regions up to the local onset of alternans, which is indicated as a red box. Fig. 2.6C shows the histograms of eigenvalues $\lambda_{[4]}$ separately for the *1:1* (black) and $1{:}1_{alt}$ (red) regions at different BCLs. Note a pronounced narrowing of the histogram and clustering around a mean value of -0.84±0.01, as we approach B^{onset} in the $1{:}1_{alt}$ region. Similar, but less pronounced behavior occurs in the *1:1* region, with some clustering around the mean value of -0.73±0.01, as we approach B^{onset}.

2.4.4 Eigenvalue Progression with BCL

One way of predicting alternans at i.e. determining the BCL at which alternans occurs would be calculating a single average eigenvalue at each BCL and look for trends if any, found in these eigenvalues by tracing them over decreasing BCLs unto the BCL where alternans occurred(B^{onset}).

The mean values of the eigenvalues $\lambda_{[4]}$ from Fig. 2.6B are shown in Fig. 2.7 for different BCLs both for *1:1* (filled circles) and *1:1$_{alt}$* (open circles) regions. Note that mean eigenvalue $\bar{\lambda}_{[4]}$ decreases as BCL decreases for both regions, although they are not statistically significant between *1:1* and *1:1$_{alt}$* regions until the onset of alternans, i.e. B^{onset}=170 ms. At the B^{onset}, the mean eigenvalues $\bar{\lambda}_{[4]}$ are statistically different ($p<0.05$) between the two regions (indicated by ***** in Fig. 2.7). These results indicate that eigenvalues $\bar{\lambda}_{[4]}$ can predict the local onset of APD alternans in the heart.

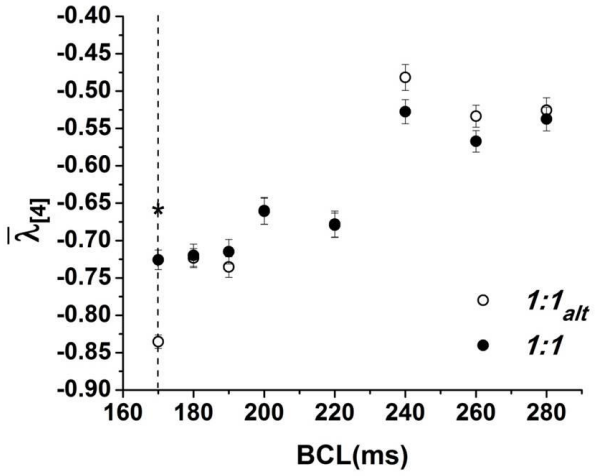

Fig. 2.7 Decreasing trend of mean eigenvalue $\bar{\lambda}_{[4]}$ with decreasing BCL is demonstrated for pixels belonging to 1:1 (filled circles) and 1:1alt (open circles) regions for one experiment with Bonset (170 ms) marked with the dashed line. * denotes statistical significance ($p<0.05$).

2.4.5 Eigenvalue at alternans Onset and comparison of $\lambda_{[2]}$ and $\lambda_{[4]}$

After observing decreasing trends in the $\lambda_{[4]}$ eigenvalue it was a natural step to see whether similar results were observed by using $\lambda_{[2]}$ (calculated using matrix $Z_{[2]}$) , the motivation being, less amount of calculations required to calculate $\lambda_{[2]}$ and to test whether just two APD measurements (APD^{90} & APD^{50}) were enough to predict local onset of alternans.

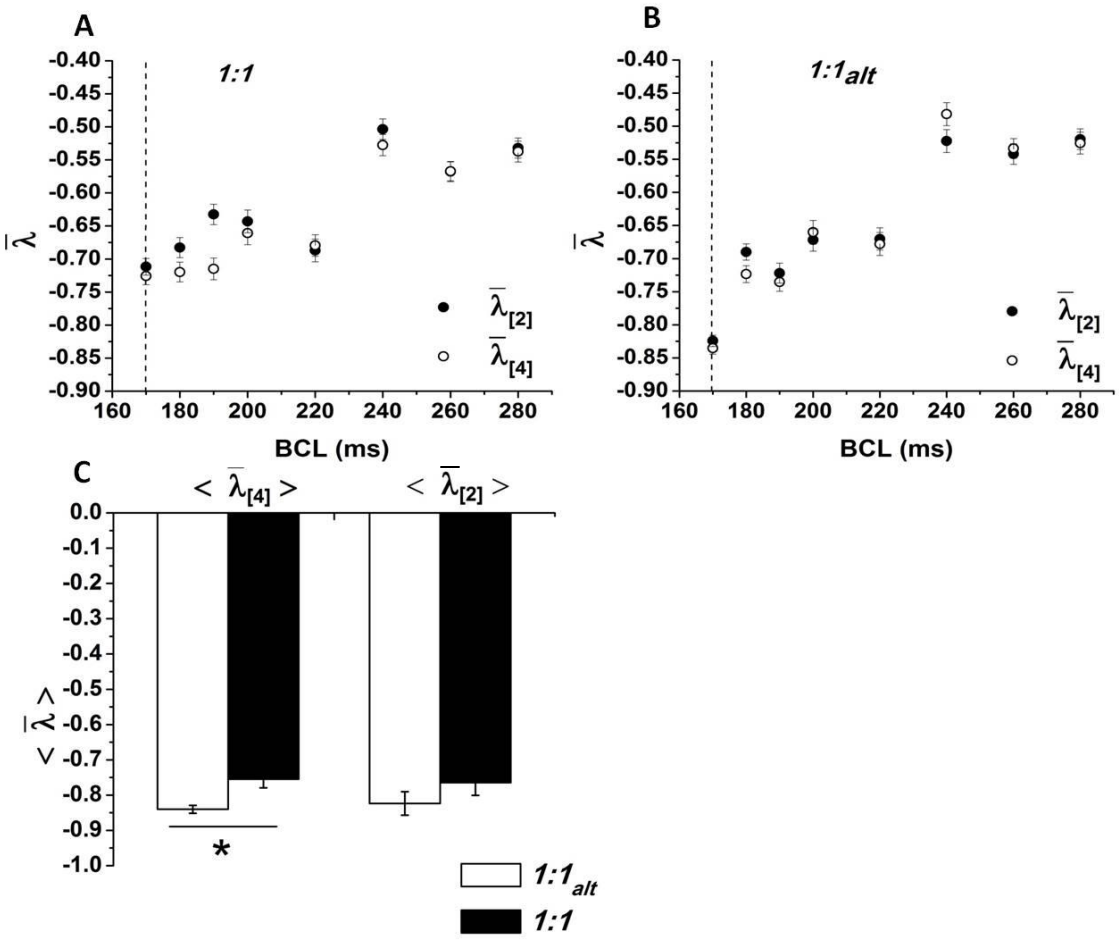

Fig. 2.8 A. Two methods of eigenvalue calculation have been compared by plotting mean eigenvalues $\bar{\lambda}_{[4]}$ (open circles) and $\bar{\lambda}_{[2]}$ (closed circles) corresponding to pixels belonging to 1:1 region for one representative experiment showing that they evaluate more or less similar values with Bonset (170 ms) denoted by dashed line. B. Similar plot for 1:1alt region for the same experiment. C. Average eigenvalues $<\bar{\lambda}_{[4]}>$ (left column pair) and $<\bar{\lambda}_{[2]}>$ (right column pair) at Bonset averaged over four experiments are shown for the 1:1 (filled bar) and the 1:1alt (open bar) regions indicating that 1:1alt region has more negative eigenvalue associated with it compared to the 1:1 region. * indicates statistical significance at $p<0.05$ level.

As a representative example, an experiment shown in Fig. 2.4 was analyzed using both methods. Fig. 2.8 illustrates the mean eigenvalues $\bar{\lambda}_{[2]}$ (filled circles) and $\bar{\lambda}_{[4]}$ (open circles) as a function of BCL both for *1:1* (Panel A) and *1:1$_{alt}$* (Panel B) regions. Our results indicate that for both regions, the two methods give statistically similar eigenvalues at all BCLs.

Next, an evaluation of whether the mean eigenvalues in all our experiments (n=4) $\bar{\lambda}_{[2]}$ and $\bar{\lambda}_{[4]}$ could predict the local onset of alternans was done. The overall average values of $\bar{\lambda}_{[2]}$ and $\bar{\lambda}_{[4]}$ viz. $<\bar{\lambda}_{[2]}>$ and $<\bar{\lambda}_{[4]}>$ calculated at the onset of alternans, B^{onset}, are shown in Fig. 2.8C separately for the *1:1* (filled) and *1:1$_{alt}$* (open) regions. Note that the mean eigenvalues $\bar{\lambda}_{[4]}$ were significantly different between *1:1$_{alt}$* (-0.84±0.01) and *1:1* (-0.76±0.02, $p<0.05$) regions. On the other hand mean eigenvalues $\bar{\lambda}_{[2]}$ did not reach statistical significance (*1:1$_{alt}$:* -0.82±0.03, and *1:1* : -0.76±0.04, p = N/S).

2.5 Conclusions and Discussion

One aim of this thesis was to predict alternans formation in the rabbit heart using a recently developed dominant eigenvalue method. I applied this technique at the whole heart level by measuring the action potential responses from data obtained in high resolution voltage mapping experiments and calculating eigenvalues from them.

2.5.1 Mean eigenvalues showed decreasing trend.

The mean eigenvalue approached -1 as the BCL was progressively decreased unto B^{onset} . This trend observed in both of eigenvalues viz. $\bar{\lambda}_{[4]}$ and $\bar{\lambda}_{[2]}$. This implies that an alternans prediction method based on eigenvalues in whole hearts is feasible. This could be done by calculating similar mean eigenvalues at each decreasing BCL and then doing a projection of these eigenvalues (using a curve fit) onto low valued BCLs to determine which one would correspond to a eigenvalue of -1. A BCL obtained in such a way would be a good guess for B^{onset}.

2.5.2 $\bar{\lambda}_{[4]}$ is better than $\bar{\lambda}_{[2]}$

Two different sets of APDs(1. APD^{90}, APD^{70}, APD^{50}, APD^{30} and 2. APD^{90}, APD^{50}) were considered to calculate the mean eigenvalues $\bar{\lambda}_{[4]}$ and $\bar{\lambda}_{[2]}$ respectively as we wanted to determine whether just two measurements were sufficient to predict the onset of alternans. However only $\bar{\lambda}_{[4]}$ was able to achieve statistical significance between the *1:1* and $1{:}1_{alt}$ regions at B^{onset} over four experiments establishing the correlation between $\bar{\lambda}_{[4]}$ and alternans onset.

$\bar{\lambda}_{[2]}$ which was calculated using just 2 measurements of the APD on the other hand wasn't able to achieve statistical significance. This may be explained by the fact that the number of dimensions required to represent the state space of heart remains unknown and just two APD measurements may fail to characterize the response.

However the mean eigenvalues evaluated over the four experiments using both the methods are very similar at B^{onset}, pointing to the possibility that the statistical insignificance for $\bar{\lambda}_{[2]}$ may be due to experimental errors in voltage mapping experiments

or the errors associated with linearizing the non-linear dynamics of the heart. $\bar{\lambda}_{[4]}$, in contrast, derived by using four measurements, succeeded in achieving the result.

Also, just four beats after short perturbation were utilized to generate the eigenvalue whereas the numerical simulations in [22] used more than ten beats which may explain why our experiments did not achieve an eigenvalue very close to -1.

2.5.3 Addressing the shortcoming of Restitution Approach

Methods based on restitution curve have not been able to fully predict the formation of alternans moreover they necessitate calculation of the slopes for a wide range of BCLs to generate a good restitution curve and use one APD measurement (for e.g. APD^{90}) to generate it.

In contrast this eigenvalue based method utilized two or more repolarization duration measurements for characterizing each AP which are then subjected to singular value decomposition to determine the most dominant dimensions. This helped in reducing the errors associated with under-characterizing the system which may occur due to single APD measurement like APD^{90}. Moreover an independent calculation of the eigenvalue at any BCL and conclusions about stability may be drawn at that particular BCL making it a curve independent approach.

As this technique gives a rough measure of the tendency of the heart to go into alternans since the eigenvalue associated with it approaches -1 as we reach B^{onset}. It may be used with changes to guide the development of a method to detect fibrillatory tendencies in the heart by considering the durations of different segments of the ECG, instead of the APDs, as significant state space variables governing the stability of the heart.

Chapter 3 Study the effects of introducing rate variability in pacing on a ionic model of a single cell.

3.1 Background

Heart rate variability refers to the observation that physiological heart rate is never constant and exhibits a variability which is said to result out of the heart rate controlling balance exercised by the parasympathetic and sympathetic nervous system. For example consider the Fig. 3.1 which was generated after ECG analysis of about one hour duration of a healthy subject. It can be easily seen in Fig. 3.1A that RR interval which is the inverse of heart rate is not constant over time. Also shown in Fig. 3.1B is a histogram of RR intervals shown in Fig. 3.1A.

HRV measures are used sometimes in clinical setting as an indicator of the health of a patient. Some measures which are HRV derived also indicate the balance between the parasympathetic and sympathetic nervous system.

Hence it is of importance to test the effect of introducing HRV in pacing protocols which are used in experiments. As cell is a basic functional unit of the heart one hopes to derive insights into the complex phenomenon of alternans formation by doing this numerical study and studying the effect of introducing rate variability on alternans formation.

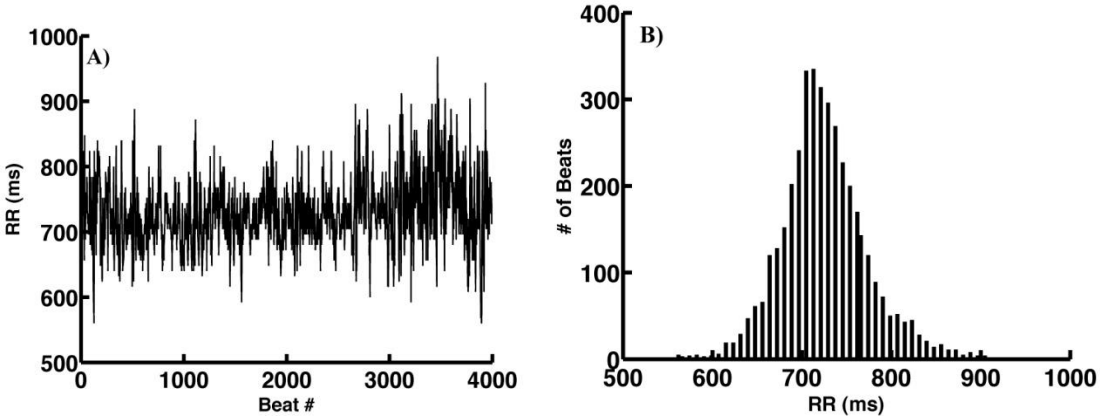

Fig. 3.1 A. A plot of RR intervals over time of a 32-year-old male with normal sinus rhythm taken from [36]. B. The histogram of the RR intervals calculated from the ECG trace shown in A.

3.2 Methods

This section deals with the ECG data analysis which was used to derive HRV measures from data sets available from PhysioNet [36] and also deals with the pacing protocols used for numerical simulations on the single cell ionic model. ECG analysis gave insights into the actual amount of HRV present under physiological conditions and similar amount of HRV was utilized in the numerical simulations.

3.2.1 ECG Data Analysis

ECG data analysis of 14 patients taken from PhysioNet database was performed. Based on the information provided in PhysioNet, the data sets were divided in two different categories: Healthy (n=8), and Diseased (n=6). All Diseased patients were diagnosed with myocardial infarction.

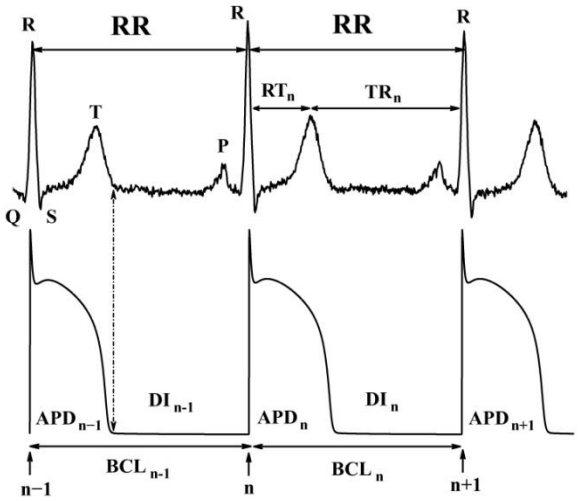

Fig. 3.2 The correspondence between APD, DI, and BCL values (cellular level) and the RT, TR, and RR intervals (whole heart level) from the ECG.

Each ECG trace was approximately 120 seconds long. Mainly band-pass filtering and peak detection approaches were used to calculate the following parameters (see Fig. 3.2): RR intervals, determined as a distance between RR peaks; standard deviation (SD_{RR}) and average (AVG_{RR}) of RR intervals; TR and RT intervals, determined as a distance between T and R peaks, and R and T peaks within RR intervals. HRV for each ECG data sets was determined as

$$HRV = \frac{SD_{RR}}{AVG_{RR}} * 100\ \% \qquad \textbf{Equation 3.1}$$

3.2.2 Pacing protocols for numerical simulations

To investigate the influences of HRV on alternans formation, a physiological ionic model of a canine cardiac action potential [35] was used. This model exhibits APD alternans while being periodically paced at progressively decreasing BCLs, and therefore, a well-defined value of BCL for the onset of alternans, BCL_{start}, and for the end of alternans, BCL_{end}, can be defined. The APD was calculated at 80% repolarization (APD^{80}).

Two different pacing protocols were used to model HRV in numerical simulations, based on ECG analysis: the variable-BCL and variable-DI protocols.

The variable-BCL pacing protocol is described by Equation 3.2 , where BCL_n = BCL. Pacing started at BCL = 400 ms, and then decreased BCL by increments of 10 ms down to 100 ms. 120 stimuli were applied at each BCL in order to reach steady state. HRV was modeled by modifying the BCL in Equation 1.1 to the following

$$BCL_n = BCL + \delta_n \qquad \textbf{Equation 3.2}$$

where δ_n is a random number with a normal distribution in the interval [-HRV*BCL, HRV*BCL], and HRV is defined by Equation 3.1. The value of HRV was varied between 0% and 6% to model the values that were seen from ECG data analysis.

In the variable-DI protocol, the DI value was held fixed, so that Equation 1.1 did not hold anymore. The DI values were set to correspond to the steady state values of DI from the variable-BCL protocol with HRV = 0%. When alternans was present in the variable-BCL protocol, the DI value was the average of two concurrent stimuli. Similar to the variable-BCL protocol, HRV was modeled as the following,

$$DI_n = DI + \delta_n \qquad \textbf{Equation 3.3}$$

where δ_n was a random number with a normal distribution either in the interval [-HRV*BCL, HRV*BCL] or in the interval [-HRV*DI,HRV*DI], where HRV was defined by Equation 3.1. The necessity of two intervals was determined by the fact that

the origin of HRV is unclear: we do not know whether HRV originates from BCL (RR interval) or the DI (TR interval).

3.2.3 Numerical Simulations

For each value of HRV, both protocols were run 10 times to mimic a stochastic process. The last 20 APDs for each BCL (or DI) for each run, representing steady state responses, were divided into even and odd beats and the mean values of $<APD>_{even}$ and $<APD>_{odd}$, and corresponding standard errors were calculated separately. For each run, alternans was defined as

$$|\Delta APD| = |\langle APD\rangle_{even} - \langle APD\rangle_{odd}| > 5ms \qquad \textbf{Equation 3.4}$$

Equation 3.4 was also used to determine the BCL at which alternans appears, BCL_{start}, and the BCL at which alternans ends, BCL_{end}, at each run. Then the mean $\langle BCL\rangle_{start}$ and $\langle BCL\rangle_{end}$ with their respective standard error were determined from the 10 runs.

Once BCL_{start} was determined at each run, a restitution curve was constructed from the last 20 APD values and DI values prior to BCL_{start}.

Statistical Analysis

Statistical significance of the ECG data, presented in Table 3.1 and Table 3.2, was determined by one-way ANOVA analysis. Data was considered statistically significant if $p<0.01$. Statistical significance of numerical data was determined using Student's t-test. Numerical results were considered statistically significant if $p<0.01$.

3.3 Results

3.3.1 ECG Analysis Results

To ensure that the HRV which would be utilized in pacing protocols was similar to the physiological observed values, ECG analysis was done, the results of which are presented below.

Patient ID	AVG_{RR} (ms)	SD_{RR} (ms)	HRV (%)
S0306	975.8	60.9	6.2
S0303	771.5	34.5	4.5
S0292	874.3	39.3	4.5
S0304	888.9	22.6	2.5
S0308	839.2	27.4	3.3
S0452	1047.5	46.0	4.4
S0457	1044.0	67.7	6.5
S0460	1113.8	69.4	6.2
AVG	944.3±42.1*	46.0±6.4*	4.8±1.5*

Table 3.1 ECG Analysis of Healthy Patients representing average RR interval (AVGRR), standard deviation of the RR interval, (SDRR), and HRV. * denotes statistical significance ($p<0.05$).

Patient	AVG_{RR} (ms)	SD_{RR} (ms)	HRV (%)
TWA18	699.7	19.6	2.8
TWA38	711.7	18.5	2.6
TWA31	710.0	13.8	1.9
TWA11	786.0	20.8	2.6
TWA20	814.8	25.7	3.2
TWA42	824.0	34.5	4.2
AVG	757.2±23.3*	22.2±2.9*	2.9±0.8*

Table 3.2 ECG Analysis of Diseased Patients , representing average RR interval (AVG_{RR}), standard deviation of the RR interval, (SD_{RR}), and HRV. * denotes statistical significance ($p<0.05$).

Comprehensive analyses of ECG traces from the two groups of patients, Healthy and Diseased, are presented in Table 3.1 and Table 3.2, respectively. Note that AVG_{RR}, (944.38±42.08 ms vs. 757.7±23.25 ms, $p<0.01$), SD_{RR}, (45.98±6.42 ms vs. 22.15±2.92 ms, $p<0.01$), and HRV (4.76±1.45% vs. 2.89±0.75%, $p<0.01$) are significantly larger for the Healthy patients in comparison with the Diseased patients.

3.3.2 Variable BCL Pacing :Effect of HRV on alternans

In order to investigate the susceptibility of the model to exhibit alternans, (i.e. the range of BCLs over which it exhibited alternans) two values of BCL, one at which alternans was first observed (BCL_{start}) and the BCL when it ceased to be (BCL_{end}) were noted. This was done at different values of HRV to test its effect on this range.

Fig. 3.3A shows APD as a function of BCL for the ionic model of an isolated cardiac myocyte that was paced using the variable-BCL protocol with no HRV (Fig. 3.3A) and HRV = 2.5% (Fig. 3.3B). Note the formation of alternans at a certain range of BCLs both with and without HRV. Also note that the onset of alternans occurred at a higher BCL (BCL_{start} = 200 ms) and ended at a lower BCL (BCL_{end} = 140 ms) for HRV = 2.5% than for HRV = 0% (BCL_{start} = 190 ms and BCL_{end} = 150 ms, respectively).

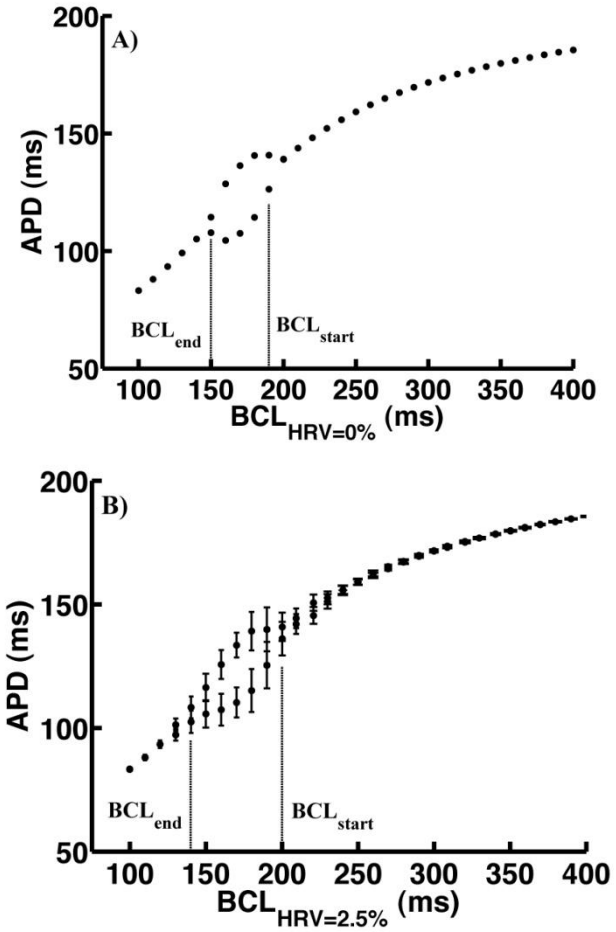

Fig. 3.3 APD as a function of BCL for the ionic model paced with variable-BCL pacing protocol with HRV = 0% (A) and 2.5% (B). BCL_{start} and BCL_{end} denote the start and end of APD alternans.

Fig. 3.4A illustrates the influence of HRV on the onset, $<BCL>_{start}$, and the end, $<BCL>_{end}$, of alternans. As HRV is increased, alternans occurred earlier in the pacing protocol and ended later in the pacing protocol. Note that HRV larger than 1.5% significantly increases $<BCL>_{start}$ when compared to HRV = 0%. Similarly, HRV larger than 2.5% significantly decreases $<BCL>_{end}$. These results suggest that HRV promotes the formation of alternans with constant-BCL pacing.

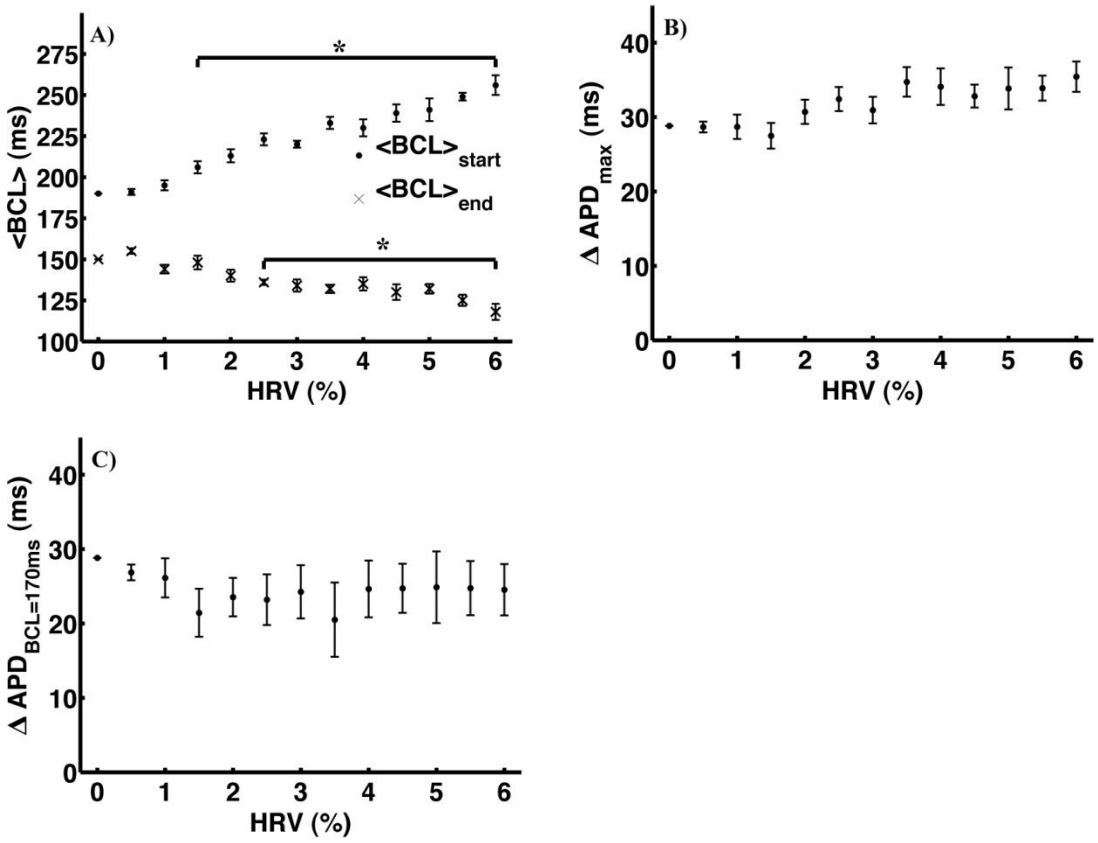

Fig. 3.4 Influence of HRV on the following parameters: A. <BCL>start and <BCL>end; B. $\Delta APD_{\max}$ **; C.** $\Delta APD_{BCL=170ms}$ *** represent statistical significance (p<0.01).**

In order to investigate the effect of HRV on the amplitude of alternans, two parameters were calculated: the maximal amplitude of alternans, $\Delta APD_{\max}$, over all BCLs in the run and the amplitude of alternans at BCL = 170 ms, $\Delta APD_{BCL=170ms}$, where alternans was present at HRV = 0%. The influence of HRV on $\Delta APD_{\max}$ and

$\Delta APD_{BCL=170ms}$ is shown in Fig. 3.4B and Fig. 3.4C, respectively. Fig. 3.4B and Fig. 3.4C show that the presence of HRV did not significantly affect either $\Delta APD_{\max}$ or $\Delta APD_{BCL=170ms}$, when compared to values at HRV = 0%.

3.3.3 Variable DI pacing: Effect of HRV on alternans

The effect of introducing heart rate variability in pacing may be different based on the way in which it is introduced (i.e. the pacing protocol used). Simulations similar to the variable BCL protocol were performed using the variable DI protocol so that the effects of the two on alternans formation could be compared.

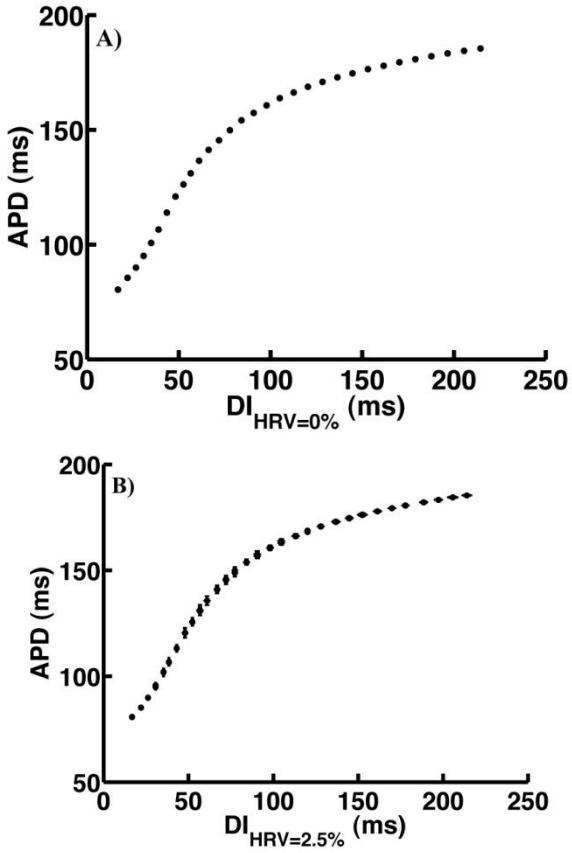

Fig. 3.5 APD as a function of DI for the ionic model paced with variable-DI pacing protocol with HRV = 0% (A) and 2.5% (B). Both figures show the absence of alternans.

Fig. 3.5 shows APD as a function of DI for the ionic model of an isolated cardiac myocyte that was paced using the constant-DI protocol with HRV = 0% (Fig. 3.5A) and HRV = 2.5% (Fig. 3.5B). In this specific case, δ_n was chosen to be within the interval [-HRV*BCL, HRV*BCL]. Note that in contrast to Fig. 3.3, no alternans is present in Fig. 3.5, both for HRV = 0% or 2.5%. To confirm these findings, HRV was increased up to 12%, and alternans was still absent (data not shown). In addition, similar simulations

were performed with δ_n in the interval [-HRV*DI, HRV*DI], and obtained similar results: no alternans was seen at any value of HRV. This demonstrated that the constant DI pacing is anti-arrhythmic.

3.4 Conclusions and Discussion

The effects of HRV on formation of alternans were investigated in physiological ionic model of a canine cardiac action potential. It was demonstrated that:

(1) HRV promoted the formation of alternans in cardiac myocytes when the variable BCL pacing was used. Specifically HRV>1.5% significantly shifted the onset of alternans towards larger BCL, but does not affect the amplitude of alternans, $\Delta APD_{\max}$ and $\Delta APD_{BCL=170ms}$

(2) Variable-DI pacing prevented the formation of alternans in cardiac myocytes.

3.4.1 HRV increased the range of BCL over which alternans occurred

It was found that in the case of variable BCL pacing, the effect of HRV is pro-arrhythmic. Fig. 3.3 shows that the introduction of HRV causes $<BCL>_{start}$ to occur sooner and $<BCL>_{end}$ to be seen later. Together, these results indicate that HRV promoted alternans formation in the cell.

3.4.2 No effect of HRV on Alternans magnitude

Numerical simulations showed that for variable-BCL pacing the maximum alternans magnitude did not change significantly when HRV was introduced. The magnitude of alternans at BCL = 170 ms did not change significantly either. This demonstrates that HRV possibly has little or no effect on the magnitude of alternans for a cardiac cell.

3.4.3 No alternans formed in case of variable-DI pacing protocol

The variable-DI pacing protocol resulted in the elimination of alternans. A possible explanation of this result is that Equation 1.2 is a deterministic equation and it would be expected that with a constant-DI value that the following APD value would be the same for each beat. Alternans is not present at any amount of HRV. This once again could be explained by Equation 1.2: for a constant-DI value, we will get a constant APD value and the slope of the restitution curve at the constant-DI determines the amount of variation seen in the APD when HRV is introduced to DI. In other words, for a fixed amount of variation in the DI, if the slope of the restitution curve were small then only a small amount of variation would be seen in the APD values whereas if the slope is large, more

variation is seen in the APD. The result of alternans elimination shows that variable-DI pacing is anti-arrhythmic.

3.4.4 Implications on whole heart

These numerical simulations pointed that increase in HRV lead to increase in range of BCL over which alternans was observed using the variable BCL protocol. However it should be borne in mind that the dynamics at the whole heart level are very complex and straight extrapolation of these results to whole heart experiments would be unwise and require actual experimentation.

The question of where HRV originates in the heart remains. These numerical simulations modeled HRV by incorporating variability in both DI and BCL, corresponding to the variability originating from the TR interval or from the RR interval, respectively. It would be of interest in future experiments to acquire ECG data during different physical activities to determine how HRV changes with heart rate.

Chapter 4 Contributions

4.1 Eigen Value Approach

- Formulation of Study.
- Implementation of code.
- Data analysis using above code.
- Manuscript preparation for submission to journal.(1st author)

4.2 HRV Approach

- Partial Formulation of Study.
- Implementation of code for ECG Analysis.
- Presentation of Initial work in 2 poster presentations.
- Manuscript review and preparation for submission to journal. (2nd author)

Chapter 5 Bibliography

[1] J. M. Pastore, S. D. Girouard, K. R. Laurita, F. G. Akar, and D. S. Rosenbaum, Circulation **99**, 1385 (1999).

[2] D. P. Zipes and H. J. Wellens, Circulation **98**, 2334 (1998).

[3] M. R. Franz, J. Cardiovasc. Electrophysiol. **14**, S140 (2003).

[4] R. J. Myerburg and P. M. Spooner, Cardiovasc. Res. **50**, 177 (2001).

[5] Z. J. Zheng, J. B. Croft, W. H. Giles, and G. A. Mensah, Circulation **104**, 2158 (2001).

[6] J. B. Nolasco and R. W. Dahlen, J. Appl. Physiol. **25**, 191 (1968).

[7] M. L. Koller, M. L. Riccio, and R. F. Gilmour Jr, Am. J. Physiol. **275**, H1635 (1998).

[8] G.M. Hall, S. Bahar, and D.J. Gauthier, Phys. Rev. Lett., **82**, 2995–2998 (1999).

[9] R. F. Gilmour Jr, J. Cardiovasc. Electrophysiol. **13**, 1150 (2002).

[10] I. Banville and R. A. Gray, J. Cardiovasc. Electrophysiol. **13**, 1141 (2002).

[11] M.R. Guevara, G. Ward, A. Shrier, L. Glass, in , 1984), p. 167.

[12] M. L. Riccio, M. L. Koller, and R. F. Gilmour Jr, Circ. Res. **84**, 955 (1999).

[13] J. I. Goldhaber, L. H. Xie, T. Duong, C. Motter, K. Khuu, and J. N. Weiss, Circ. Res. **96**, 459 (2005).

[14] C. de Diego, R. K. Pai, A. S. Dave, A. Lynch, M. Thu, F. Chen, L. H. Xie, J. N. Weiss, and M. Valderrabano, Am. J. Physiol. Heart Circ. Physiol. **294**, H1417 (2008).

[15] Q. Lou and I. R. Efimov, Conf. Proc. IEEE Eng. Med. Biol. Soc. **2009**, 4527 (2009).

[16] E. G. Tolkacheva, D. G. Schaeffer, D. J. Gauthier, and W. Krassowska, Phys. Rev. E. Stat. Nonlin Soft Matter Phys. **67**, 031904 (2003).

[17] D. Sato, Y. Shiferaw, A. Garfinkel, J. N. Weiss, Z. Qu, and A. Karma, Circ. Res. **99**, 520 (2006).

[18] A. R. Cram, H. M. Rao, and E. G. Tolkacheva, Biophys. J. **100**, 868 (2011).

[19] S. H. Strogatz, *Nonlinear Dynamics and Chaos* (Cambridge, Westview, CO, 1994).

[20] N. F. Otani, M. Li, and R. F. Gilmour Jr, Heart Rhythm **2**, 1261 (2005).

[21] M. Li and N. F. Otani, Ann. Biomed. Eng. **31**, 1213 (2003).

[22] A. Petrie and X. Zhao, Proceedings of the Royal Society A: Mathematical, Physical and Engineering Science **468**, 3649-3666 (2012).

[23] J. Jackson, *A user's guide to principal components.* (John Wiley & Sons, New York, NY, 1991).

[24] Y. Shiferaw, M. A. Watanabe, A. Garfinkel, J. N. Weiss, and A. Karma, Biophys. J. **85**, 3666 (2003).

[25] J. J. Fox, E. Bodenschatz, and R. F. Gilmour Jr, Phys. Rev. Lett. **89**, 138101 (2002).

[26] R. F. Gilmour Jr, N. F. Otani, and M. A. Watanabe, Am. J. Physiol. **272**, H1826 (1997).

[27] N. F. Otani and R. F. Gilmour Jr, J. Theor. Biol. **187**, 409 (1997).

[28] E. M. Cherry and F. H. Fenton, Am. J. Physiol. Heart Circ. Physiol. **286**, H2332 (2004).

[29] J. N. Weiss, A. Karma, Y. Shiferaw, P. S. Chen, A. Garfinkel, and Z. Qu, Circ. Res. **98**, 1244 (2006).

[30] S. Mironov, J. Jalife, and E. G. Tolkacheva, Circulation **118**, 17 (2008).

[31] P. V. Bayly and L. N. Virgin, Proceedings of the Royal Society of London. Series A: Mathematical and Physical Sciences **443**, 391 (1993).

[32] J. J. Batzel and H. T. Tran, J. Math. Biol. **41**, 45 (2000).

[33] www.homeheart.co.uk

[34] R. Arora, M. K. Das, D. P. Zipes, and J. Wu, Indian. Pacing Electrophysiol. J. 3, 187 (2003).

[35] J. J. Fox, J. L. McHarg, and R. F. Gilmour Jr, Am. J. Physiol. Heart Circ. Physiol. 282, H516 (2002).

[36] G. B. Moody, R. G. Mark, and A. L. Goldberger, Conf. Proc. IEEE Eng. Med. Biol. Soc. 2011, 8327 (2011).

[37] J. N. Weiss, A. Garfinkel, H. S. Karagueuzian, Z. Qu, and P. S. Chen, Circulation 99, 2819 (1999).

[38] www.snl.salk.edu- Tutorial on Principal Component Analysis.

Chapter 6 Appendix

6.1 Eigenvalue calculation from time series data: Theory

Say **X**(t) is the state vector representing the state of the system and the system's dynamics are governed by

$$\frac{dX}{dt} = \boldsymbol{f}(X) \qquad \textbf{Equation 6.1}$$

where $\boldsymbol{f}$ is a vector function.

Let the solution to Equation 6.1 be given by $\phi(\boldsymbol{X}, t)$ where $\phi(\boldsymbol{X}, t)$ is the trajectory of the system in time, which essentially determines the value of state variables at any time instant and hence the system's behavior is completely defined.

In our case, the heart, a periodic behavior is observed at the cellular and the whole organ level which manifests as an almost constant HR over short time intervals.

We wish to explore whether the heart's state space can be defined by various action potential measurements. Since these action potentials have a periodic nature, we can define the state variables once every cycle, making our system discrete.

Consider a discrete solution to the continuous case $\phi(X_0, nT)$ where X_0 is the initial state vector and X_n is the state vector at the nth cycle. Thus we have

$$X_1 = \phi(X_0, T)$$
$$X_2 = \phi(X_1, T)$$

and so on. In general $X_n = P(X_{n-1})$ where $\phi(X, T) = P(X)$ where P is a mapping function.

The stability of periodic solution ϕ is based on stability of X^*,a fixed point on this trajectory.

Linearizing the dynamics near X^* we have

$$X_n \approx \nabla P \cdot X_{n-1}$$
$$X_{n-1} \approx \nabla P \cdot X_{n-2} \qquad \textbf{Equation 6.2}$$
$$\vdots$$
$$X_1 \approx \nabla P \cdot X_0$$

Thus $X_n = (\nabla P)^n \cdot X_0$

Say $\nabla P = Q\Lambda Q^{-1}$ after eigenvalue decomposition .

$Q = [q_1\ q_2\ q_3\ \cdots\ q_k]$

where q_i is the i[th] column of Q.

Thus

$$X_n \approx (Q\Lambda Q^{-1})^n \cdot X_0$$
$$\Rightarrow X_n \approx Q\Lambda^n Q^{-1} \cdot X_0$$
$$\therefore X_n \approx Q\Lambda^{\mathrm{n}}\mathrm{c} \qquad \textbf{Equation 6.3}$$

where $c = Q^{-1}X_0$ and $c = [c_1 c_2 \cdots c_k]'$

$$X_n = Q\Lambda^{\mathrm{n}}\mathrm{c} + \delta_{\mathrm{n}}$$

where δ_n is the error in linearizing Equation 6.3 .

$$\therefore X_n = q_1\lambda_1^n c_1 + q_2\lambda_2^n c_2 + q_3\lambda_3^n c_3 + \cdots + q_k\lambda_k^n c_k \qquad \textbf{Equation 6.4}$$

λ_i is a diagonal element of matrix Λ which are the eigenvalues.

The most dominant eigenvalues determine the stability.

Say these eigenvalues are $\lambda_1, \lambda_2, \lambda_3 \cdots \lambda_m\ m \leq k$ then

$$X_n = q_1\lambda_1^n c_1 + q_2\lambda_2^n c_2 + q_3\lambda_3^n c_3 + \cdots + q_m\lambda_m^n c_m + \psi_n \qquad \textbf{Equation 6.5}$$

where ψ_n incorporates errors due to linearization of map P as well as the process of restricting the number of dominant eigenvalues to m.

Let us denote the final result as below.

$$X_n = \bar{Q}\bar{\Lambda}^n\bar{c} + \psi_n \qquad \textbf{Equation 6.6}$$

If X_n is measurable q_i and λ_i can be determined by least squares method, however X_n being a true state space variable, it cannot be measured directly and hence we need to

introduce a relation between the measured state space variables (Y_n) and the true state space variables (X_n).

Let this relation be given by R.

Thus

$$Y_n \approx RX_n \qquad \textbf{Equation 6.7}$$

Equation 6.6 and Equation 6.7 imply that

$$Y_n = R\bar{Q}\bar{\Lambda}^n\bar{c} + R\psi_n \qquad \textbf{Equation 6.8}$$

$$Y_n = R\bar{Q}\bar{\Lambda}^n\bar{c} + \xi_n$$

where ξ incorporates all errors up to this point.

We can write Equation 6.8 in the expanded form as below:

$$y_n = y_* + \lambda_1^n v_1 + \lambda_2^n v_2 + \cdots + \lambda_m^n v_m + \xi_n \qquad \textbf{Equation 6.9}$$

where y_n is the measured state variable vector at the n^{th} beat and y_* is the steady state response and v_i are columns.

6.2 Principal Component Analysis

Principal component analysis (**PCA**) is a method of determining the most dominant dimensions in a data set in terms of the maximum information conveyed. Maximum information is conveyed when the variance associated with the dimension is high.

Say for example the trajectory data of a particle moving in 3 dimensions, is given to us. If this trajectory is plotted we see that the trajectory is helix shaped, however the helix is almost flat and that the particle does not move much in the Z direction. A principal component analysis of this trajectory data will inform us that the particle dynamics is effectively limited to the X-Y plane as well as give us perpendicular vectors (**basis/axes**) on which the particle's trajectory can be projected to represent the data in this new system.

These basis vectors are so designed that the variance of co-ordinates of the particle's trajectory along each of these new axes is minimized. Thus in this example PCA will help us identify that the particle's trajectory is essentially in the X-Y plane. In most of its applications PCA helps in redundancy reduction and when applied to experimental measurements it results in error reduction and thus results in a high signal to noise ratio.

Steps involved in PCA [38]:

Data Matrix:

Let $X_{m\times n}$ be the data matrix where n denotes the number of measurements and m denotes the number of dimensions.

$$X = [x_1 x_2 x_3 \cdots x_n]$$

where x_i is a column of the matrix X and corresponds to one set of measurements of co-ordinates. It is also to be noted that the mean is subtracted from all the rows i.e. we subtract the means from all the measurements in any particular dimension.

Co-variance Matrix:

The covariance matrix is denoted by C_X and defined as

$$C_X = X \cdot X^T$$ **Equation 6.10**

This matrix is a good indicator of the degree of relatedness of measurements in any particular dimension to the any other dimension. C_X reflects the noise and redundancy in measurements. The diagonal terms, when they have large values, correspond to an interesting structure in the data. In the off-diagonal terms large magnitude corresponds to high amount of redundancy in the data.

Diagonalization of the Co-variance Matrix:

The whole process of PCA is to obtain the dominant dimensions in the data and thereby reduce the variance in any of the identified principal dimensions.

Let us say that C_Y is such an optimal co-variance matrix which is obtained by representing the data matrix X by Y in a different system of coordinates (i.e. different basis vectors). Our objectives while determining a transformation to make this projection from X to Y is directed by our aim to make the diagonal elements as high as possible and making the off-diagonal elements as small as possible.

Let P be this projection matrix such that

$$PX = Y$$ **Equation 6.11**

To determine P we need to determine its columns $p_1, p_{2,}, p_3 \cdots p_m$which is in fact the new basis (orthonormal). Orthogonality ensures that the off diagonal elements are nullified. Also note that more the variance associated with p_i in the new co-variance matrix C_Y more important it is(i.e. more principal it is.)

Determination of P :

$$C_Y = Y \cdot Y^T$$ **Equation 6.12**

From, Equation 6.10, 6.11 & 6.12 we get

$$C_Y = PC_XP^T \qquad \textbf{Equation 6.13}$$

Since C_X is a symmetric matrix, it can be diagonalized.

say,

$$C_X = EDE^T \qquad \textbf{Equation 6.14}$$

where E is a matrix containing the eigenvectors of C_X as columns and D is a diagonal matrix.

Now if we select P to be E^T i.e. eigenvectors of C_X are rows of P .

By substituting Equation 6.13 in Equation 6.14 we have

$$C_Y = P[EDE^T]P^T$$
$$\therefore C_Y = P[P^TDP]P^T$$
$$\therefore C_Y = (PP^T)D(PP^T)$$
$$\therefore C_Y = (PP^{-1})D(PP^{-1})$$

as P is an orthogonal matrix implies $P^T = P^{-1}$.

$$C_Y = D \qquad \textbf{Equation 6.15}$$

Thus a choice of $P = E^T$ diagonalizes C_X .

We thus conclude that he eigenvectors of C_X are the principal components of the data X and thus an eigenvector calculation of C_X gives us required projection matrix.

6.3 Application of PCA to calculate eigenvalues with example:

As mentioned in the section "EigenValue Calculation using Time Series Data" least squares method can be used to estimate eigenvalues. However the problem is twofold we need to determine the number of dominant eigenvalues and their actual magnitudes as well at the same time.

Example:

Let us suppose that our state space comprises of 3 dominant variables (dimensions) viz. APD^{90}, APD^{70} and APD^{50} (identified by PCA) with the corresponding eigenvalues λ_1, λ_2 and λ_3. According to Equation 6.9 we have

$$APD_n^{90} = APD_*^{90} + v_{APD^{90},1} \cdot \lambda_1^n + v_{APD^{90},2} \cdot \lambda_2^n + v_{APD^{90},3} \cdot \lambda_3^n \quad \text{Equation 6.16}$$

$$APD_n^{70} = APD_*^{70} + v_{APD^{70},1} \cdot \lambda_1^n + v_{APD^{70},2} \cdot \lambda_2^n + v_{APD^{70},3} \cdot \lambda_3^n \quad \text{Equation 6.17}$$

$$APD_n^{50} = APD_*^{50} + v_{APD^{50},1} \cdot \lambda_1^n + v_{APD^{50},2} \cdot \lambda_2^n + v_{APD^{50},3} \cdot \lambda_3^n \quad \text{Equation 6.18}$$

where APD_n^k represents APD at k% repolarization and n denotes the beat number similarly v_{APD^k} is the vector corresponding to k% repolarization.

Writing Equation 6.16, 6.20 and 6.21 in matrix form we have:

$$y_n = y_* + C \cdot [\lambda_1^n \quad \lambda_2^n \quad \lambda_3^n]' \quad \text{Equation 6.19}$$

where

$y_n = [APD_n^{90} \quad APD_n^{70} \quad APD_n^{50}]'$

$y_* = [APD_*^{90} \quad APD_*^{70} \quad APD_*^{50}]'$ and $C = \begin{bmatrix} v_{APD^{90},1} & v_{APD^{90},2} & v_{APD^{90},3} \\ v_{APD^{70},1} & v_{APD^{70},2} & v_{APD^{70},3} \\ v_{APD^{50},1} & v_{APD^{50},2} & v_{APD^{50},3} \end{bmatrix}$

Now if $v_{APD^{90}}$, $v_{APD^{70}}$ and $v_{APD^{50}}$ are not perfectly correlated then C is invertible we can write Equation 6.19 as

$$y_n - y_* = C \cdot \begin{bmatrix} \lambda_1 & 0 & 0 \\ 0 & \lambda_2 & 0 \\ 0 & 0 & \lambda_3 \end{bmatrix} \cdot C^{-1} \cdot C \cdot \begin{bmatrix} \lambda_1^{n-1} \\ \lambda_2^{n-1} \\ \lambda_3^{n-1} \end{bmatrix} \qquad \textbf{Equation 6.20}$$

Substituting $n = n - 1$ in Equation 6.19 we have

$$y_{n-1} - y_* = C \cdot [\lambda_1^{n-1} \quad \lambda_2^{n-1} \quad \lambda_3^{n-1}]' \qquad \textbf{Equation 6.21}$$

Combining Equation 6.19, 6.20 and 6.21 we have

$$y_n - y_* = D \cdot (y_{n-1} - y_*) \qquad \textbf{Equation 6.22}$$

where $D = C \cdot \Lambda \cdot C^{-1}$.

By definition of similar matrices the eigenvalues of D are λ_1, λ_2 and λ_3.

Now our task is to estimate D from available measurements.

Say $\{y_n\}_{n=1}^{N}$ is a series of measurements from action potentials. Let us define

$$Y_1 = [y_1 - y_* \quad \cdots \quad y_{N-1} - y_*] \qquad \textbf{Equation 6.23}$$

$$Y_2 = [y_2 - y_* \quad \cdots \quad y_N - y_*] \qquad \textbf{Equation 6.24}$$

From Equation 6.22 , 6.23 and 6.24 we have

$$Y_2 = D \cdot Y_1 \qquad \textbf{Equation 6.25}$$

We can estimate D from Y_1 and Y_2 using least squares giving us

$$D = [Y_2 Y_1^T] \cdot [Y_1 Y_1^T]^{-1} \qquad \textbf{Equation 6.26}$$

Thus, if we know the number of dominant eigenvalues or the dominant dimensions and have the corresponding measurements the matrix D can be estimated by least squares method and the eigenvalues calculated.

Calculation of Y_1 and Y_2 from measurements:

Say we have a data matrix Z with the data from N beats with each beat having 7 measurements viz. APD^{90}, APD^{80}, APD^{70}, APD^{60}, APD^{50}, APD^{40} and APD^{30} populated in it.

$$Z = \begin{bmatrix} APD_1^{90} - APD_*^{90} & \cdots & APD_1^{30} - APD_*^{30} \\ \vdots & \ddots & \vdots \\ APD_N^{90} - APD_N^{90} & \cdots & APD_N^{30} - APD_*^{30} \end{bmatrix} \quad \text{Equation 6.27}$$

Now we determine the dominant dimensions using PCA or using singular value decomposition which is another method of dominant dimension identification. Let us say that the dominant dimensions turn out to be the ones corresponding to APD^{90}, APD^{70} and APD^{50}. We construct another matrix given below which has data only from the dominant dimensions:

$$\bar{Z} = \begin{bmatrix} APD_1^{90} - APD_*^{90} & APD_1^{70} - APD_*^{70} & APD_1^{50} - APD_*^{50} \\ \vdots & \vdots & \vdots \\ APD_N^{90} - APD_N^{90} & APD_N^{70} - APD_N^{70} & APD_N^{50} - APD_*^{50} \end{bmatrix} \quad \text{Equation 6.28}$$

Now from Equation 6.23, 6.24 and 6.28 we have

$$Y_1 = [\,\bar{Z}_1{}', \cdots, \bar{Z}_{N-1}{}'\,] \quad \text{Equation 6.29}$$

$$Y_2 = [\,\bar{Z}_2{}', \cdots, \bar{Z}_N{}'\,] \quad \text{Equation 6.30}$$

where $\bar{Z}_i{}'$ is the i^{th} row of $\bar{Z}$.

Once Y_1 and Y_2 are known D can be obtained by Equation 6.26 and the eigenvalues calculated.